ADVANCED MATERIALS
www.advmat.de

Decoupled Solar Energy Storage and Dark Photocatalysis in a 3D Metal–Organic Framework

*Philip M. Stanley, Florian Sixt, and Julien Warnan**

Materials enabling solar energy conversion and long-term storage for readily available electrical and chemical energy are key for off-grid energy distribution. Herein, the specific confinement of a rhenium coordination complex in a metal–organic framework (MOF) unlocks a unique electron accumulating property under visible-light irradiation. About 15 C g_{MOF}^{-1} of electric charges can be concentrated and stored for over four weeks without loss. Decoupled, on-demand discharge for electrochemical reactions and H_2 evolution catalysis is shown and light-driven recharging can be conducted for >10 cycles with ≈90% of the initial charging capacity retained. Experimental investigations and theoretical calculations link electron trapping to MOF-induced geometry constraints as well as the coordination environment of the Re-center, highlighting the key role of MOF confinement on molecular guests. This study serves as the seminal report on 3D porous colloids achieving photoaccumulation of long-lived electrons, unlocking dark photocatalysis, and a path toward solar capacitor and solar battery systems.

1. Introduction

Natural photosynthesis aptly combines harvesting and storing solar energy in chemical bonds via water oxidation and carbohydrate formation by comparting the overall redox reaction in photosystems I and II.[1] While water oxidation is light-driven, the Calvin–Benson–Bassham cycle is a "dark process" (i.e., light-independent) that converts extracted electrons to carbohydrates as energy carriers.[2] Artificially mimicking such a decoupled model for photoelectric conversion and electron storage would provide off-grid solutions to society's rapidly growing yet intermittent energy needs.[3] While considerable progress has been achieved in storing photovoltaic-cell-generated electrochemical potential in decentralized batteries,[4] or by solar fuel production,[5] one ideal, less energy-loss- and implementation-cost-associated approach would combine photoconversion, energy storage, and controlled release abilities within one solar rechargeable system.[6] For "wireless" particular systems in solution, such properties have been previously reported for graphene-, or carbon-nitride-based materials, however, the longevity of stored charges in these examples does not surpass one day,[7–9] rendering efficient off-grid energy delivery practically challenging. Additional unmet prerequisites toward cost-competitive solar batteries/capacitors include high efficiencies and stabilities paired with low raw material and processing costs.

Metal–organic frameworks (MOFs) are crystalline materials built from metal-based nodes and coordinating organic linkers, forming networks with permanent porosity.[10] Their combinatorial versatility has enabled hallmark energy-related advances, e.g., as supercapacitors,[11] water-splitting materials,[12] or battery separators.[13] Interfacing these 3D matrices with discrete coordination complexes adds a further level of material design sophistication, inspired by intricate biological systems, with examples in solar fuel production,[14,15] light-driven oxidations,[16] and dye-sensitized solar cells.[17]

Herein, we show that functionalizing an Al node-based MOF-253 with a rhenium Lehn-type molecular complex,[18–20] yields a hybrid material that intakes, accumulates, and stores electric charges under visible-light irradiation in presence of an electron source (**Figure 1**). 15 C g_{MOF}^{-1} were accumulated in 1.5 h of irradiation with a solar-to-output energy conversion and storage efficiency (η) of ≈0.9% and stored over four weeks with negligible loss. A rechargeable electron storage and delivery behavior was shown with ≈1% capacity loss per cycle. This contrasts with previously reported homogeneous Re molecular catalysts and Re-based hybrids (including covalent organic frameworks, metal oxides, and polymers) that conversely display catalytic activity.[19,21–23] This unique behavior was characterized and quantified by electron paramagnetic resonance (EPR), UV–vis, and attenuated total reflectance infrared (ATR-IR) spectroscopy, paired with density functional theory (DFT) calculations. Its origin was linked to the impact of the confinement from the porous colloids on the Re-center's molecular reactivity. To the best of our knowledge, this off-grid system represents a seminal account of long-lived electron accumulation and

P. M. Stanley, F. Sixt, J. Warnan
Chair of Inorganic and Metal-Organic Chemistry
Department of Chemistry, and Catalysis
Research Center (CRC)
TUM School of Natural Sciences
Technical University of Munich
Garching, Germany
E-mail: julien.warnan@tum.de

The ORCID identification number(s) for the author(s) of this article can be found under https://doi.org/10.1002/adma.202207280.

DOI: 10.1002/adma.202207280

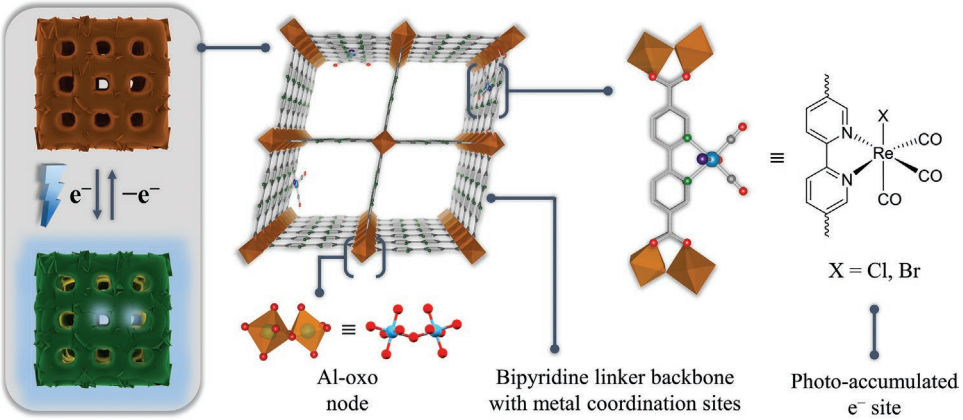

Figure 1. Schematic light-induced charge and dark discharge of the electron-accumulator and structural representation of its building blocks (i.e., Al-oxo nodes and 5,5'-dicarboxy-2,2'-bipyridine linkers). The bipyridine coordination sites are loaded with Re centers. Red: O, Cyan: Al, Green: N, Grey: C, Blue: Re, Purple: X.

photo-rechargeability in MOFs or 3D highly porous materials. Finally, upon coupling with an ancillary electrocatalyst, this charge can be released on-demand to drive delayed, dark H_2 evolution catalysis, thereby decoupling light-dependent and -independent reactions and yielding a scheme toward tackling the intermittency of solar irradiation.

2. Results and Discussion

2.1. Material Synthesis and Characterization

Pristine MOF-253 was synthesized solvothermally from modified literature procedures (details in Supporting Information) using $AlCl_3$ and 5,5'-dicarboxy-2,2'-bipyridine (5,5'-dcbpy) linkers.[24] The vacant 2,2'-bipyridine (bpy) sites were loaded by soaking MOF-253 powders in an acetonitrile (MeCN) solution of $ReX(CO)_5$ (X = Cl, Br) at 65 °C for 24 h, yielding $ReCl(CO)_3$@MOF-253 (**ReCl-253**) or $ReBr(CO)_3$@MOF-253 (**ReBr-253**) (Figure 1; Table S1, Supporting Information).

Also matching simulated patterns of single crystals, powder X-ray diffraction (PXRD) patterns were obtained unaltered after loading of the Re centers, suggesting that the MOF crystallinity was not affected (**Figure 2**a).

N_2 adsorption measurements showed high gas uptake and a Brunauer–Emmett–Teller (BET) surface area of around 1250 $m^2\ g^{-1}$ for MOF-253, while uptake was reduced by about 70% upon functionalization (Figure 2a,b; Figure S1 and S2, Supporting Information).[25] The decrease in the pore size volume of MOF-253's calculated (rectangular) 13 Å-pores is rationalized by introduced Re centers and trapped solvents due to the low sample activation temperatures (T) employed to avoid damaging the Re complex. Elemental analysis estimated around 11 wt% Re, corresponding to approximatively 1 in 10 bpy linkers occupied by the Re complex (Table S2, Supporting Information). Higher Re precursor weigh-ins resulted in similar loadings, suggesting MOF saturation, potentially limited by modest pore diffusion and steric hindrance from immobilized Re centers, rendering the inner crystallite volume inaccessible.[26] ATR-IR spectra for loaded MOFs displayed distinct bands at 1917 and 2023 cm^{-1}, not present for pristine MOF-253, which are characteristic of the $Re(CO)_3$ moiety (Figure 2c).[27] The corresponding solid-state UV–vis measurements showed a broad new band between 370 and 600 nm, comparable to $ReBr(CO)_3$(5,5'-dcbpy)'s absorption and mirrored by a powder color change from white to dark orange, allowing visible light absorption (Figure 2d; Figure S3, Supporting Information). Scanning electron microscopy (SEM) visualized crystal morphology and particle sizes of 1.05 ± 0.35 µm for pristine MOF-253 and **ReCl-253** samples, and energy-dispersive X-ray (EDX) mapping showed a homogeneous Re distribution within the material (Figures S4–S8, Supporting Information). The pristine MOF-253 was temperature-stable up to $T \approx 400$ °C.[20] The thermostability decreased upon Re loading, rationalized by the more labile $Re(CO)_3$ unit (Figure S9, Supporting Information). Together, these data provide strong evidence for successful $ReX(CO)_3$ center incorporation into MOF-253.

2.2. Photoinduced Electron-Accumulation

fac-[$ReX(CO)_3$(bpy)]-based materials are well-documented CO_2-to-CO photocatalysts, operating with or without an external photosensitizer due to their visible-light absorption properties (Figures 2d; Figures S3 and S10, Supporting Information).[19,21–23] However, **ReCl-253** and **ReBr-253** powders suspended in dry MeCN with triethanolamine (TEOA) as a sacrificial electron donor (SED) yielded no detectable CO, $HCOO^-$, H_2, or CH_4 (probed by gas chromatography and ^1H nuclear magnetic resonance (NMR) spectroscopy) under irradiation at 450 nm (Tables S3 and S4, Supporting Information). Conversely, a stark powder color change from orange to dark green was observed (Figure S11-S12). Variation of the solvent (MeCN, pentane or *N*,*N*-dimethylformamide (DMF)), CO_2- or argon-saturated atmosphere and substituting TEOA for 1,3-dimethyl-2-phenyl-2,3-dihydro-*1H*-benzo[*d*]imidazole (BIH) all resulted in similar green color and no CO_2 conversion (Table S5, Supporting Information).[28] Adding water yielded no green coloration with marginal CO evolution below catalytic values.[29] Control experiments with pristine (Re-free) MOF-253, no irradiation

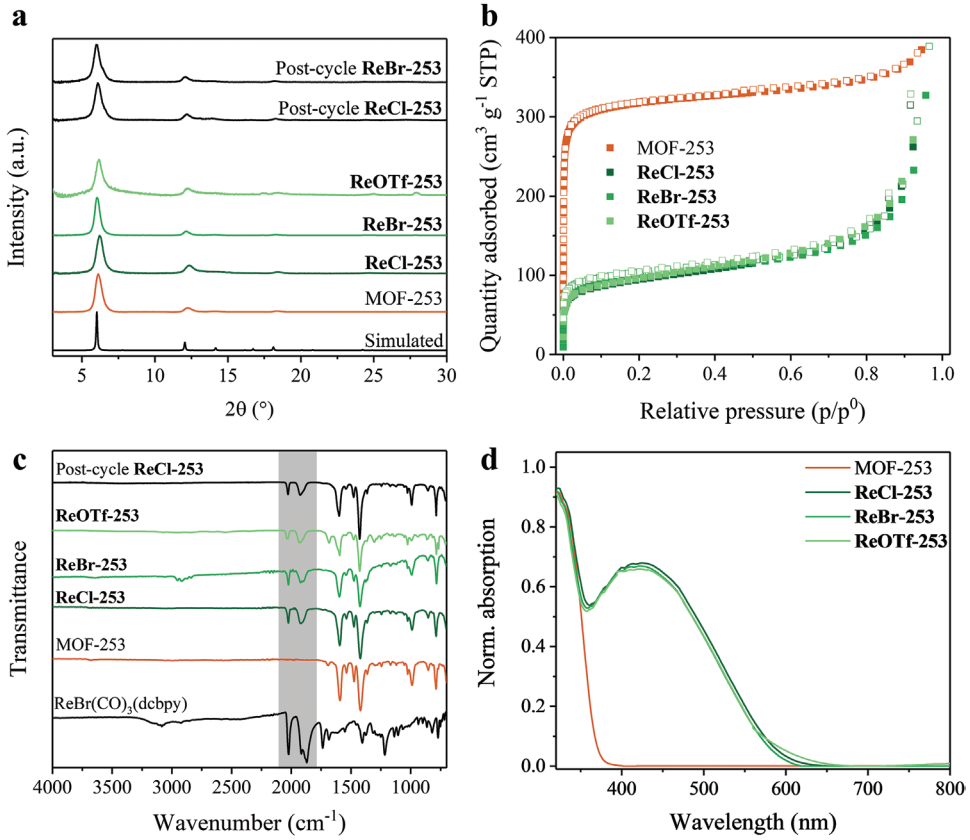

Figure 2. Characterization of pristine and loaded MOF-253 samples. a) PXRD patterns, including simulation from single crystal data (CCDC 691 979).[20] b) N_2 adsorption isotherms at 77 K. c) ATR-IR spectra with the ν_{CO} region of "$Re(CO)_3$" highlighted. d) Solid-state UV–vis spectra.

or no TEOA yielded no color change and no detected product formation, whereas testing $ReBr(CO)_3$(5,5'-dcbpy) in homogeneous conditions produced turnover numbers (TONs) ≈20 (Table S3, Supporting Information). These observations suggest that a MOF-specific CO_2-independent photoredox reaction occurs at Re centers. This is consistent with typically observed reductive quenching of the $ReX(CO)_3$(bpy) excited state by TEOA/BIH, yielding a ligand-localized radical, but contrasts with the anticipated subsequent X^- dissociation enabling CO_2-to-CO conversion (Figure S10, Supporting Information).[18,30,31]

The green powders were isolated and further studied under the exclusion of air as the latter triggers a return to the original color (Figure S3). EPR spectroscopy unambiguously revealed paramagnetic species with $g = 2.0034$ for **ReCl-253** and $g = 2.0047$ for **ReBr-253** (**Figure 3**a; Figure S13, Supporting Information). The g values paired with the broad signal and absence of hyperfine coupling suggest free electrons.[32] Here, the serendipity of the metal–organic network's low conductivity (acting as an insulator) and bpy-Re centers' electroactivity likely confines the free electrons to the $ReX(CO)_3$(5,5'-dcbpy) units.

Solid-state UV–vis spectra showed a new band at $\lambda = 650$ nm (Figure 3b; Figure S14, Supporting Information), matching features obtained by DFT calculated time-dependent (TD) UV–vis on $[ReCl(CO)_3(5,5'\text{-dcbpy})]^{\bullet-}$ fragments in the MOF-253 equivalent (details in Supporting Information, wB97xD/LANL2DZ level, Figures S15 and S16, Supporting Information). This ascription is in-line with one-electron-reduced species monitored as transient species in prior spectroscopy reports.[31,33] Additionally, we performed DFT geometry optimizations and TD-DFT UV–vis calculations on two fragments after Cl^- loss, and potential solvent (MeCN) coordination, respectively (Figure S10, Supporting Information). In accordance with the above ascription, the corresponding calculated absorptions feature predominantly around 550 and 800 nm (in line with comparable reports on $[Re(CO)_3(bpy)]$-based complexes) and do not match the observed UV–vis band (Figure 3b; Figure S17 and S18, Supporting Information).[34,35]

ATR-IR spectra of the green powders extracted from the various dry photocatalytic media (recorded under air exclusion) in the solvent-free ν_{CO} region revealed comparable bands to pre-irradiation with a general 5 cm^{-1} shift to lower wavenumbers, and an additional shoulder at 1897 cm^{-1} (Figure 3c; Figure S19, Supporting Information). Similar growth was reported under homogeneous electrocatalysis and assigned to a bipyridine-based reduction of the complex species,[36] and the ν_{CO} band shifts are ascribed to π-backbonding changes between the Re and the carbonyl ligands as the electron density of the metal cation increases.[37] The small shifts compared to prior reports presumably stem from a rigidified MOF-induced environment, moderate electronic distribution over the Re orbitals, and incomplete reduction of the bpy-Re centers. No band loss or a strong shift from 2023 cm^{-1} to below 2000 cm^{-1} (from Cl^-/Br^- ligand dissociation or MeCN/solvent adduct formation, respectively) was observed, highlighting the stability of the reduced

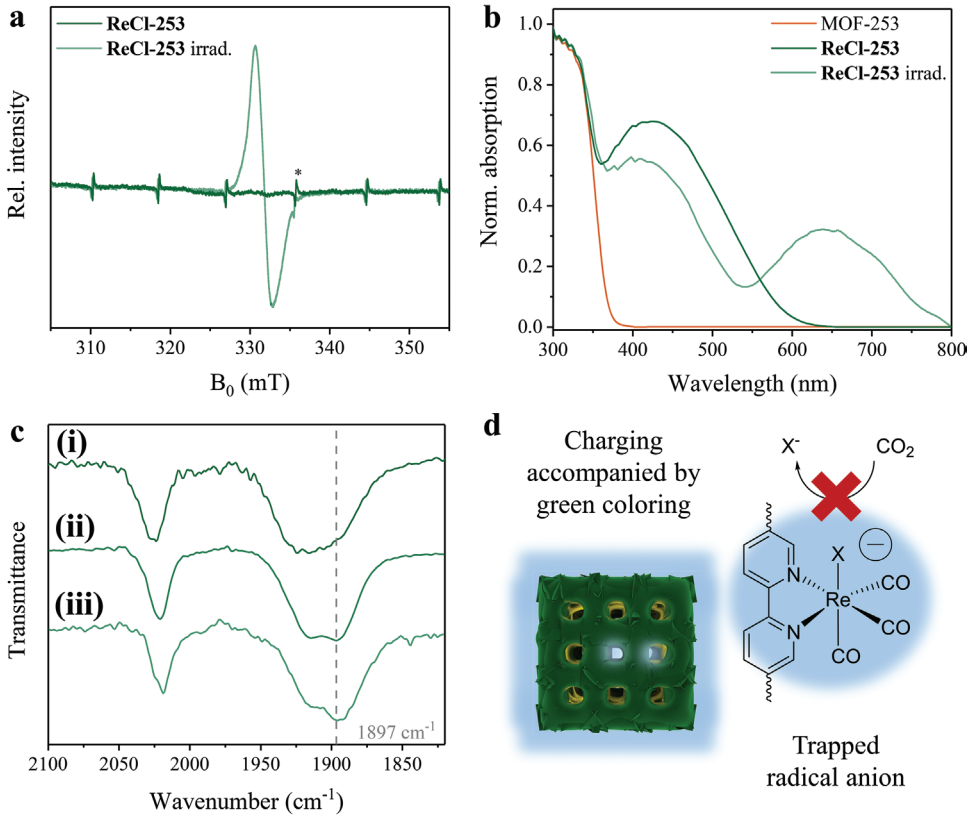

Figure 3. Characterization of **ReCl-253**'s properties after exposure to 450 nm irradiation in organic media with an electron donor. a) Solid-state EPR spectra ($g = 2.0034$). *Mn^{2+} reference. b) Solid-state UV–vis spectra. c) ATR-IR spectra of (top to bottom) as-synthesized **ReCl-253** (i), samples charged in MeCN with Ar atmosphere (ii), and MeCN with BIH instead of TEOA (iii). d) MOF/molecular radical anion formation and stabilization scheme.

species.[38,39] Additionally, ν_{Re-Cl} vibrations around 340 cm^{-1} for **ReCl-253** showed retained signals for the irradiated green powder, that are not present for pristine MOF-253 but are also visible in the precursor $ReCl(CO)_5$ (Figure S20, Supporting Information).[40,41] Adding an excess of $AgNO_3$ to a post-irradiation solution to promote hypothetical AgCl formation and precipitation revealed no Cl^- ions in the solution as no particles were detected by dynamic light scattering measurement (Figure S21, Supporting Information).

Overall, these analyses support that Re-complex excitation is followed by reductive quenching forming thermodynamically stable radical anions, as $[ReCl(CO)_3(5,5'\text{-dcbpy})]^{\bullet-}$ fragments, without triggering X^- dissociation (Figure 3d). Protons from water traces or SED degradation likely act as the countercations to maintain charge balance. Remarkably, the insulating network of the MOF together with the anchoring here enables the isolation of the reactive radicals that would typically result in compound degradation in molecular systems.[31]

2.3. Radical Trapping Investigation

Next, we investigated the origin of radical trapping and its longevity in Re-loaded MOF-253 samples. We ran DFT calculations and optimized the $[ReCl(CO)_3(5,5'\text{-dcbpy})]^{\bullet-}$ fragment as a discrete complex, as well as integrated into MOF-253 and UiO-67 by using the corresponding literature-extracted single crystal linker structures with fixed node-coordinating oxygen atoms to simulate the rigidifying MOF environment (Figure S22, Supporting Information). Bpy-based and *fac*-$[ReX(CO)_3(bpy)]$-functionalized UiO-67 was chosen as a representative MOF benchmark due to numerous photocatalytic CO_2 reduction reports.[15,42,43] Major differences were observed in the five-membered ring and bipyridyl angles as the frameworks affect the complex's geometry (Table S6, Supporting Information). For MOF-253, bipyridyl dihedral (NCCN torsion) and in-plane bending angles depict planar coordination and low bipyridyl unit distortion with the discrete and UiO-67-counterparts featuring bent and twisted conformations (**Figure 4**a; Figure S22, Supporting Information).[44] Accordingly, calculated energy levels are higher for the discrete complex, followed by UiO-67- and MOF-253-based materials (−3.25, −3.41, and −3.74 eV, respectively). This contrasts with the opposite trend observed for the neutral species (Table S7, Supporting Information). While fully understanding the steric situation is complex, these results tentatively suggest that the unrestrained discrete system is able to freely relax to a lower energy minimum in the ground state while the MOFs likely stabilize the reduced radical complex due to a pre-imposed conformation. The electronic density localization of the single-occupied molecular orbital (SOMO) is in all cases mainly ligand-centered, albeit with a lower distribution on the Re center for the MOF-253 complex (Figure 4a; Figure S23, Supporting Information) in line with increased bipyridyl electron density delocalization. These imply

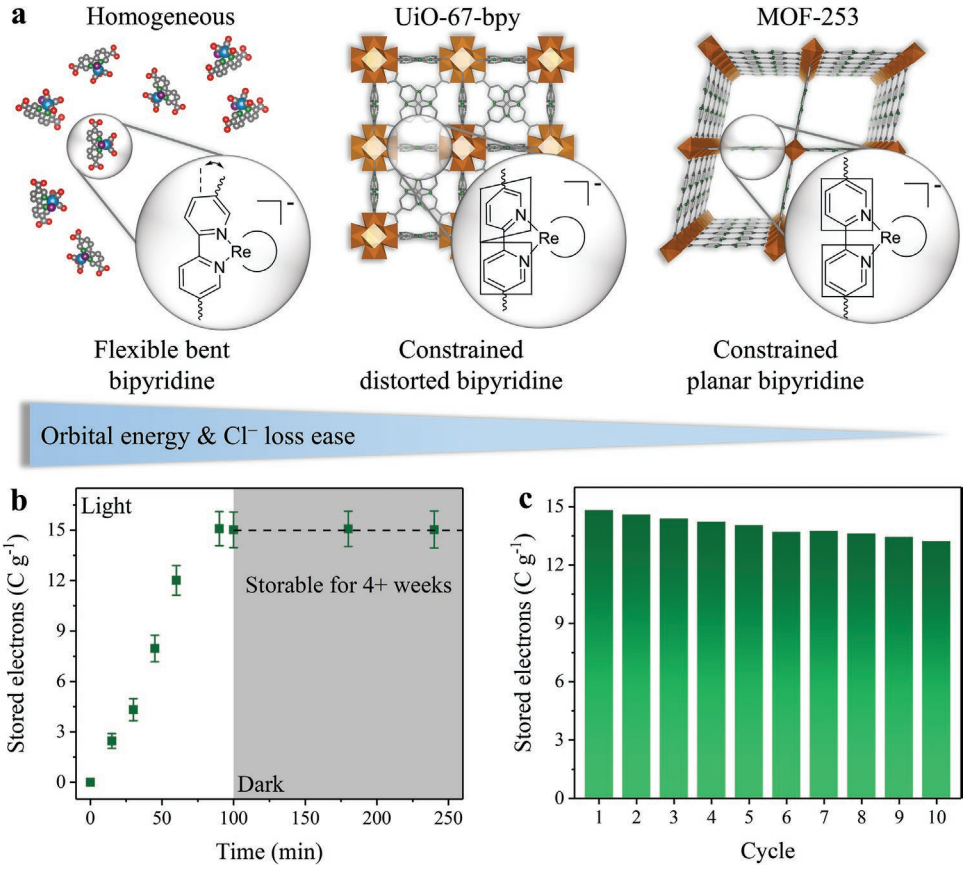

Figure 4. a) Environment-induced $[ReCl(CO)_3(5,5'\text{-dcbpy})]^{\bullet-}$ DFT-calculated geometry, contributing to stabilization in MOF-253 via reduced SOMO orbital energy and Cl^- ligand loss ease. b) Stored electrons based on irradiation time (450 nm in MeCN with TEOA) and charge storage in the dark. Values are means with standard deviation from three replicates under identical conditions. c) Stored charges per charging and discharging cycle (under Ar in MeCN with TEOA).

a lower reactivity and a higher electrophilicity of the Re atom in $ReCl(CO)_3(5,5'\text{-dcbpy})^{\bullet-}$ of MOF-253, likely deterring ligand dissociation and stabilizing the radical anion.

To further support our hypothesis, we investigated replacing chloro/bromo ligand for triflate (OTf) as a ligand with a stronger nucleofuge character.[45] The $Re(OTf)(CO)_5$ precursor was synthesized and reacted with MOF-253, yielding $Re(OTf)(CO)_3$@MOF-253 (**ReOTf-253**) (Table S1, Supporting Information). Assembly characterizations were found comparable to **ReCl-253** and **ReBr-253**, with additional ATR-IR bands between 1000 and 1350 cm^{-1}, similar to $Re(OTf)(CO)_5$ and indicative of successful OTf inclusion (Figure 2a–d; Figure S24, Table S2, Supporting Information). In contrast to **ReCl-253** and **ReBr-253**, applying **ReOTf-253** in standard CO_2 reduction conditions yielded clear catalytic behavior with detectable CO (TONs with BIH ≈35, Figures S25 and S26, Table S3, Supporting Information), as well as alteration of the $Re(OTf)(CO)_3$ unit post-catalysis as evidenced by ATR-IR spectroscopy (Figure S27, Supporting Information). Experiments performed with $^{13}CO_2$ for **ReOTf-253** confirmed CO_2 as the sole source of CO and the catalytic reaction nature (Figure S28, Supporting Information).[46] The catalytic activity is in line with previous reports on homogeneous $ReX(CO)_3(bpy)$-based complexes showing that increased ligand lability (from Cl to Br to OTf) promotes ligand de-coordination, unlocking catalytic activity. Conversely, the more electrophilic the Re atom is, the less likely it is to de-coordinate an anionic ligand.[47] Paired with our experiments, this affirms that the electron density distribution is responsible for inducing electro-catalysis or -accumulation behaviors, and highlights the "conditioning" impact from MOF-253's confinement on the Re complex's electronic properties and performance. For MOF systems, this agrees well with the reactivity trend shown by a CO_2-to-formate RhCl-bpy-based catalyst upon integration in various porous solids (including UiO-67 and MOF-253) with different electron-donating/withdrawing effects.[48]

2.4. Electron Storage and Controlled Release

Next, we examined the electron storage abilities of our hybrid materials. Charging and discharging experiments were conducted. After a given irradiation time (at λ = 450 nm, MeCN/TEOA 20/1 v/v, Ar-degassed) the light source was switched off and an Ar-purged methyl viologen dichloride (MV) solution was injected into the green colloidal mixture under air exclusion. This resulted in an immediate solution blue coloring together with the return of the MOF's orange color, indicating

rapid electron transfers from the MOF to MV.[49,50] UV–vis spectroscopy and Lambert–Beer analysis after various irradiation times determined the reduced MV concentrations and, correspondingly, the electron quantities stored in the corresponding green powders (details in the Supporting Information). Electrons were consistently accumulated over a 90 min irradiation period before reaching the maximum charge of 15.1 ± 1.0 and 11.5 ± 0.9 C g_{MOF}^{-1} (4.2 and 3.2 mA h g_{MOF}^{-1}, 0.045 and 0.032 C m^{-2}) for **ReCl-253** and **ReBr-253**, respectively (Figure 4b, Figures S29–S32, Tables S8–S10, Supporting Information). These values were confirmed by quantitative EPR analysis (Figure S13, Supporting Information). Considering metal loadings from elemental analysis (Table S2, Supporting Information), ≈26% and 21% of Re centers for **ReCl-253** and **ReBr-253**, respectively, are estimated to be reduced at full charge (supported by UV–vis analysis see Figure S16, Supporting Information), possibly limited by the maximum charge density and SED diffusion.[51] For **ReCl-253**, if all bpy sites were loadable with a Re center and those were in-turn all charged, the maximum charge density could reach an impressive value of ≈545 ± 34 C g_{MOF}^{-1} (≈1.6 C m^{-2}, assuming the surface area remains unchanged). This provides a perspective for future material optimization to unlock the full electron-accumulation potential. ATR-IR spectra and PXRD patterns measured after discharging matched pre-charging species, suggesting molecular integrity and global framework retention (Figure 2a,c). Doubling the incident light intensity per area by switching from monochromatic 450 nm LEDs to a bandpass filter tailored to the Re complex absorption (λ = 400–500 nm) enabled full-charging in 60 min (Figures S33 and S34, Supporting Information). Moving to the edge of the materials' absorption band by irradiating with 520 or 600 nm LEDs significantly reduced the charging rate, confirming the Re complex as the origin of the light sensitization (Figure 2d; Figure S35, Supporting Information). Additionally, doubling the TEOA concentration (to increase the probability of the bimolecular reaction to quench the excited Re state) and halving the weigh-in of MOF particles (reducing scattering and increasing the light available per Re center), also increased the charging speed (Figure S36, Supporting Information). Together, these experiments show that the radical charging rate can be modulated by the irradiation intensity and component concentrations toward optimized fast-charging applications.

ReCl-253's charge/discharge stability was probed under Ar atmosphere in MeCN with TEOA (Figure 4c; Figure S37, Table S11, Supporting Information) revealing a ≈1% average capacity loss per cycle and ≈11% loss after 10 cycles. Capacity loss is ascribed to gradual pore filling/blocking over subsequent cycles with TEOA/MV/solvent molecules rendering Re centers inaccessible, as suggested by a modest porosity decrease in the post-cycling N_2 adsorption isotherms (Figures S38 and S39, Supporting Information). While this is not competitive with recent state-of-the-art photocapacitors with >95% retained capacity after thousands of cycles,[52] it serves as an apt proof-of-principle demonstration for MOF-based materials.

Besides performance, other parameters such as stability, synthetic yield, scalability, and costs are key toward device applicability. Our material showed chemical stability by crystallinity and Re molecular unit retention in various solvents (MeCN, pentane, DMF, and H_2O) (Figures S40 and S41, Supporting Information) as well as tolerance to irradiation conditions. Based on low-cost and heavy-metal free $AlCl_3$ and the off-the-shelf linker 5,5'-dcbpy, MOF-253 can be synthesized in high yields (85% of pristine activated MOF, see Supporting Information), affording a promising candidate toward sustainable and affordable synthesis scaling.[53] However, an alternative to the precious metal Re-based site should be developed to reduce costs and increase practicability. Additionally, replacing TEOA by an expendable feedstock source such as biomass, plastics, food waste, or building block chemicals may enable sustainability, photoreforming reactions, and avenues toward chemical synthesis (e.g., alcohol to aldehyde oxidation).[54–56]

Photocharging and subsequent electron storage unlocks routes toward decoupled light and dark processes and off-grid on-demand release for electricity production and time-delayed "dark photocatalysis". As a model reaction, we examined organic dye dark degradation by injecting methylene blue (MB) or methyl orange (MO) into a suspension of charged **ReCl-253** or **ReBr-253** (details in Supporting Information).[57] While MO absorption (λ_{max} = 416 nm) remained unaffected, MB's color instantly faded as shown with UV–vis spectroscopy, indicating quantitative degradation (Figures S42 and S43, Supporting Information). In turn, quantitative MO degradation can be achieved by injecting an un-degassed MO solution, hinting at a multistep reaction starting with O_2 reduction, followed by chemical degradation of MO by reactive oxygen species.[57,58] Control experiments with uncharged **ReCl-253** and Re-free MOF-253 samples showed no dye degradation, confirming accumulated electrons as the degradation source (Figures S44 and S45, Supporting Information). Next, dark photocatalysis—i.e., a combination of a light-dependent and a delayed "dark" catalytic reaction—was attempted toward producing hydrogen. $Co(dmgH)_2$(4-COOH-py) (dmgH = dimethylglyoxime, py = pyridine), a benchmark H_2 evolution catalyst, in aqueous MeCN was added to charged **ReCl-253**.[59,60] A rapid disappearance of the green coloration of the MOF—dependent on the concentration of added catalyst—was observed together with H_2 evolution (Figure S46, Table S12, Supporting Information). At low Co catalyst concentrations (≈1.9 nmol mL^{-1}), about 72 µmol g_{MOF}^{-1} of H_2 was catalytically evolved ($TONs_{Co}$ ≈ 22) in 40 min, corresponding to around 14 C g_{MOF}^{-1}, i.e., 95% of the stored electrons. Note that the 5% shortfall is due to the initial reduction of Co(III) to Co(II) required before the catalytic cycle occurs.[61]

These demonstrate that selective and rapid use of the stored electrons is possible, proceeding via an outer sphere electron transfer to substrates that do not require a free coordination site on the rhenium atom (**Figure 5**, S10). With E_{red}(MB), E_{red}(MV), $E_{red}(O_2)$, and E_{red}(Co(dmgH)$_2$(4-COOH-py)) ≈ −0.40, −0.45, −0.57, −0.47 V vs normal hydrogen electrode (V_{NHE}), respectively,[57,60,62] the accumulated electrons' potential is highly reductive in line with ReCl(CO)(5,5'-dcbpy)'s E_{red} recorded at −0.68 V_{NHE} in homogeneous conditions, opening a path toward electrocatalytic applications.[63]

Remarkably, upon storing the charged **ReCl-253** away from light and air for 4 weeks, an identical green coloring was observed and comparable ATR-IR and EPR spectra were recorded, highlighting both the extremely long-lived nature of the trapped electrons and their tamed, yet extractable,

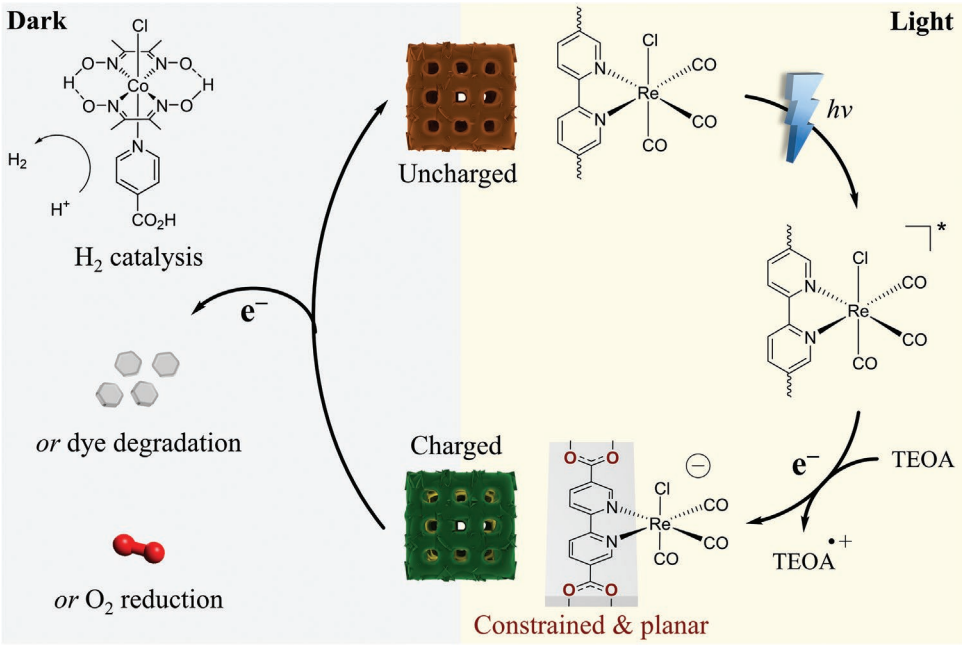

Figure 5. Working principle of decoupled light-induced charge and dark discharge of the **ReCl-253** electron-accumulator. The constraining effect of MOF-253 on Re centers conditions electronic properties enabling long-lived electron storage. On-demand use of stored charges is possible by outer sphere electron transfer to a cobaloxime-based H_2 evolution catalyst, an organic dye effecting degradation, or O_2.

proclivity (Figure S27, S47, and S48, Supporting Information). Conversely, storage at elevated temperatures (45 °C) resulted in a fast capacity loss (Figure S49, Supporting Information). Assuming 100% of stored electrons were converted into MV^{-}, a conservative emitted-photon-to-stored-electron-to-discharged-electron total efficiency value, η, of 0.9% at $\lambda = 450$ nm was calculated (Tables S8–S10, Supporting Information) as a mid-range value compared to state-of-the-art photocapacitive materials.[3]

In summary, our material shows advantages: i) as an all-in-one wireless system combining light harvesting and electron storage, ii) in the long-lived nature of stored charges, iii) by relying on an amenable 3D modular assembly principle with implications toward confinement effects, and iv) in upholding 3D porosity during charge–discharge cycles. Such electron charging and storage under irradiation have also been observed in other colloids such as 2D graphene and carbon nitride or in Ti MOF nodes with similar performance. However, these appeared unstable and only on the 12–24 h-scale storage lifetime.[7–9,64] Aside from colloids, state-of-the-art photocapacitor devices typically interface solar cells with capacitive materials such as metal oxides, metal sulfides, carbon/silicon-based compounds, or perovskites, and deliver higher performances.[65] Yet, our unoptimized system holds potential for high gravimetric charge density, with the 550 C g_{MOF}^{-1} theoretical capacity limit directly competing with state-of-the-art performance, while concomitantly opening alternative perspectives toward stand-alone wireless applications.[8,65] Future steps toward coupling the stored electrons with electronic devices include electrode fabrication—ensuring conductive contact and long-term stability in working conditions,[66] and investigating optimal charging conditions.[8]

3. Conclusion

Our hybrid system combines the elementary steps of light harvesting, photoinduced free-electron generation, and their storage in one easily made wireless material rendering photoelectrochemical configurations avoidable.[67] We showed that up to 15 C g_{MOF}^{-1} are accumulated under visible-light irradiation, which can be discharged and recharged with 1% capacity loss per cycle. Critical toward energy distribution and addressing solar irradiation intermittency, electrons were stored without a noticeable loss for a month. Conversely, they can be released on demand to drive redox reactions and H_2 production catalysis. This constitutes a rare example of decoupled, off-grid, photoelectrochemical energy storage and release, thus mimicking dark and light cycles characteristic of natural photosynthesis. Experimental observations and theoretical calculations revealed that the electron storage property originates from a confinement effect of MOF-253 on Re centers, creating a unique complex geometry and conditioned electronic properties. This phenomenon is MOF-253-specific and does not occur in discrete molecular systems, nor was observed in previously reported porous matrices (MOF and COFs).

We believe this original report on MOF-based storage of solar energy as inert radicals opens numerous avenues for new energy porous materials toward solar battery/capacitor devices. Future research opportunities and challenges include device integration (electrode fabrication) and electrical energy production (paired with cost and limitation analysis), wireless electrochemistry, using sustainable electron sources, improved charging and discharging features and stability. Concomitantly, it highlights the possibilities offered by MOFs toward synergizing host confining spaces and guests. The latter is key for

the MOF and molecular catalyst communities and may motivate the visionary goal of tailor-made reticular designs and confinement effects to stabilize excited/reactive molecular states in matrices.

4. Statistical Analysis

Source data were obtained from the respective characterization device (see Supporting Information for details) and plotted as received without further manipulation with OriginPro 2019b by OriginLab Corp. Exceptions are PXRD data and solid-state UV–vis spectra that were normalized prior. Additionally, N_2 isotherm and BET data processing were performed with 3Flex Software Version 5.01 by Micromeritics Instrument Corp.

All capacitance (C g^{-1}) values are presented as means ± standard deviation, obtained from three replicates under identical conditions. Formulas and examples for all calculations are contained in the Supporting Information.

Supporting Information

Supporting Information is available from the Wiley Online Library or from the author.

Acknowledgements

This work was supported by the German Research Foundation (DFG) Priority Program 1928 "Coordination Networks: Building Blocks for Functional Systems", the research project MOFMOX (grant number: FI 502/43-1), and by the Excellence Cluster 2089 "e-conversion" (Fundamentals of Energy Conversion Processes). P.M.S. thanks the Chemical Industry Fonds (FCI) for a Ph.D. fellowship. The authors thank Katia Rodewald for SEM images and EDX measurements, as well as Oksana Storcheva for EPR measurements. Proofreading by Jan Berger and Sarah Dummert is gratefully acknowledged, as are support and helpful discussions with Roland Fischer and Bernhard Rieger.

Open access funding enabled and organized by Projekt DEAL.

Conflict of Interest

The authors declare no conflict of interest.

Data Availability Statement

The data that support the findings of this study are available from the corresponding author upon reasonable request.

Keywords

confinement effects, dark photocatalysis, electron storage, metal–organic frameworks, solar energy conversion

Received: August 10, 2022
Revised: September 20, 2022
Published online: November 14, 2022

[1] D. Gust, T. A. Moore, *Science* **1989**, *244*, 35.
[2] J. A. Bassham, A. A. Benson, M. Calvin, *J. Biol. Chem.* **1950**, *185*, 781.
[3] Q. Zeng, Y. Lai, L. Jiang, F. Liu, X. Hao, L. Wang, M. A. Green, *Adv. Energy Mater.* **2020**, *10*, 1903930.
[4] J. B. Goodenough, K.-S. Park, *J. Am. Chem. Soc.* **2013**, *135*, 1167.
[5] D. G. Nocera, *Acc. Chem. Res.* **2017**, *50*, 616.
[6] D. Schmidt, M. D. Hager, U. S. Schubert, *Adv. Energy Mater.* **2016**, *6*, 1500369.
[7] R. Liu, C. Liu, S. Fan, *J. Mater. Chem. A* **2017**, *5*, 23078.
[8] F. Podjaski, J. Kröger, B. V. Lotsch, *Adv. Mater.* **2018**, *30*, 1705477.
[9] V. W.-H. Lau, D. Klose, H. Kasap, F. Podjaski, M.-C. Pignié, E. Reisner, G. Jeschke, B. V. Lotsch, *Angew. Chem., Int. Ed.* **2017**, *56*, 510.
[10] H. Furukawa, K. E. Cordova, M. O'Keeffe, O. M. Yaghi, *Science* **2013**, *341*, 1230444.
[11] D. Sheberla, J. C. Bachman, J. S. Elias, C.-J. Sun, Y. Shao-Horn, M. Dincă, *Nat. Mater.* **2017**, *16*, 220.
[12] H. Hu, Z. Wang, L. Cao, L. Zeng, Z. Cankun, W. Lin, C. Wang, *Nat. Chem.* **2021**, *13*, 358.
[13] S. Bai, X. Liu, K. Zhu, S. Wu, H. Zhou, *Nat. Energy* **2016**, *1*, 16094.
[14] X. Feng, Y. Pi, Y. Song, C. Brzezinski, Z. Xu, Z. Li, W. Lin, *J. Am. Chem. Soc.* **2020**, *142*, 690.
[15] P. M. Stanley, J. Haimerl, C. Thomas, A. Urstoeger, M. Schuster, N. B. Shustova, A. Casini, B. Rieger, J. Warnan, R. A. Fischer, *Angew. Chem., Int. Ed.* **2021**, *60*, 17854.
[16] X. Feng, Y. Pi, Y. Song, Z. Xu, Z. Li, W. Lin, *ACS Catal.* **2021**, *11*, 1024.
[17] W. A. Maza, A. J. Haring, S. R. Ahrenholtz, C. C. Epley, S. Y. Lin, A. J. Morris, *Chem. Sci.* **2016**, *7*, 719.
[18] J. Hawecker, J.-M. Lehn, R. Ziessel, *J. Chem. Soc., Chem. Commun.* **1983**, *9*, 536.
[19] G. Sahara, O. Ishitani, *Inorg. Chem.* **2015**, *54*, 5096.
[20] I. Senkovska, F. Hoffmann, M. Fröba, J. Getzschmann, W. Böhlmann, S. Kaskel, *Microporous Mesoporous Mater.* **2009**, *122*, 93.
[21] Z. Fu, X. Wang, A. M. Gardner, X. Wang, S. Y. Chong, G. Neri, A. J. Cowan, L. Liu, X. Li, A. Vogel, R. Clowes, M. Bilton, L. Chen, R. S. Sprick, A. I. Cooper, *Chem. Sci.* **2020**, *11*, 543.
[22] H.-P. Liang, A. Acharjya, D. A. Anito, S. Vogl, T.-X. Wang, A. Thomas, B.-H. Han, *ACS Catal.* **2019**, *9*, 3959.
[23] P. M. Stanley, J. Warnan, *Energies* **2021**, *14*, 4260.
[24] P. Valvekens, E. D. Bloch, J. R. Long, R. Ameloot, D. E. de Vos, *Catal. Today* **2015**, *246*, 55.
[25] F. Carson, S. Agrawal, M. Gustafsson, A. Bartoszewicz, F. Moraga, X. Zou, B. Martín-Matute, *Chem. - Eur. J.* **2012**, *18*, 15337.
[26] P. M. Stanley, M. Parkulab, B. Rieger, J. Warnan, R. A. Fischer, *Faraday Discuss.* **2021**, *231*, 281.
[27] A. Vlček, in *Photophysics of Organometallics*, (Eds.: A. J. Lees, F. N. Castellano), Springer, New York **2010**, p. 115.
[28] X.-Q. Zhu, M.-T. Zhang, A. Yu, C.-H. Wang, J.-P. Cheng, *J. Am. Chem. Soc.* **2008**, *130*, 2501.
[29] X. Deng, J. Albero, L. Xu, H. García, Z. Li, *Inorg. Chem.* **2018**, *57*, 8276.
[30] P. M. Stanley, C. Thomas, E. Thyrhaug, A. Urstoeger, M. Schuster, J. Hauer, B. Rieger, J. Warnan, R. A. Fischer, *ACS Catal.* **2021**, *11*, 871.
[31] S. Meister, R. O. Reithmeier, M. Tschurl, U. Heiz, B. Rieger, *ChemCatChem* **2015**, *7*, 690.
[32] M. D. Peeks, C. E. Tait, P. Neuhaus, G. M. Fischer, M. Hoffmann, R. Haver, A. Cnossen, J. R. Harmer, C. R. Timmel, H. L. Anderson, *J. Am. Chem. Soc.* **2017**, *139*, 10461.
[33] Y. Tamaki, K. Watanabe, K. Koike, H. Inoue, T. Morimoto, O. Ishitani, *Faraday Discuss.* **2012**, *155*, 115.
[34] E. Fujita, J. T. Muckerman, *Inorg. Chem.* **2004**, *43*, 7636.
[35] M. Wang, T. Weyhermüller, E. Bill, S. Ye, K. Wieghardt, *Inorg. Chem.* **2016**, *55*, 5019.

[36] C. W. Machan, M. D. Sampson, S. A. Chabolla, T. Dang, C. P. Kubiak, *Organometallics* **2014**, *33*, 4550.
[37] D. A. Kurtz, K. R. Brereton, K. P. Ruoff, H. M. Tang, G. A. N. Felton, A. J. M. Miller, J. L. Dempsey, *Inorg. Chem.* **2018**, *57*, 5389.
[38] E. E. Benson, C. P. Kubiak, *Chem. Commun.* **2012**, *48*, 7374.
[39] F. P. A. Johnson, M. W. George, F. Hartl, J. J. Turner, *Organometallics* **1996**, *15*, 3374.
[40] W. A. McAllister, A. L. Marston, *Spectrochim Acta A Mol Biomol Spectrosc* **1971**, *27*, 523.
[41] G. Diaz, A. H. Klahn, *Spectrosc. Lett.* **1990**, *23*, 87.
[42] C. Wang, Z. Xie, K. E. deKrafft, W. Lin, *J. Am. Chem. Soc.* **2011**, *133*, 13445.
[43] K. M. Choi, D. Kim, B. Rungtaweevoranit, C. A. Trickett, J. T. D. Barmanbek, A. S. Alshammari, P. Yang, O. M. Yaghi, *J. Am. Chem. Soc.* **2017**, *139*, 356.
[44] M. Bazargan, M. Mirzaei, A. Franconetti, A. Frontera, *Dalton Trans.* **2019**, *48*, 5476.
[45] M. B. Smith, J. March, *Advanced Organic Chemistry*, John Wiley & Sons, Hoboken, NJ, USA **2007**.
[46] R. Das, S. Chakraborty, S. C. Peter, *ACS Energy Lett.* **2021**, *6*, 3270.
[47] M. L. Clark, P. L. Cheung, M. Lessio, E. A. Carter, C. P. Kubiak, *ACS Catal.* **2018**, *8*, 2021.
[48] F. M. Wisser, P. Berruyer, L. Cardenas, Y. Mohr, E. A. Quadrelli, A. Lesage, D. Farrusseng, J. Canivet, *ACS Catal.* **2018**, *8*, 1653.
[49] T. Watanabe, K. Honda, *J. Phys. Chem.* **1982**, *86*, 2617.
[50] M. Heyrovský, *J. Chem. Soc., Chem. Commun.* **1987**, 1856.
[51] B. A. Johnson, A. M. Beiler, B. D. McCarthy, S. Ott, *J. Am. Chem. Soc.* **2020**, *142*, 11941.
[52] W.-Y. Jin, M. M. Ovhal, H. B. Lee, B. Tyagi, J.-W. Kang, *Adv. Energy Mater.* **2021**, *11*, 2003509.
[53] P. A. Julien, C. Mottillo, T. Friščić, *Green Chem.* **2017**, *19*, 2729.
[54] D. Antón-García, E. E. Moore, M. A. Bajada, A. Eisenschmidt, A. R. Oliveira, I. A. C. Pereira, J. Warnan, E. Reisner, *Nat. Synth.* **2022**, *1*, 77.
[55] F. Wang, D. Ouyang, Z. Zhou, S. J. Page, D. Liu, X. Zhao, *J. Energy Chem.* **2021**, *57*, 247.
[56] C. T. Uekert, C. M. Pichler, T. Schubert, E. Reisner, *Nat. Sustainability* **2021**, *4*, 383.
[57] Y.-H. Chiu, T.-F. Chang, C.-Y. Chen, M. Sone, Y.-J. Hsu, *Catalysts* **2019**, *9*, 430.
[58] M. U. D. Sheikh, G. A. Naikoo, M. Thomas, M. Bano, F. Khan, *New J. Chem.* **2016**, *40*, 5483.
[59] D. Dolui, S. Khandelwal, P. Majumder, A. Dutta, *Chem. Commun.* **2020**, *56*, 8166.
[60] A. Panagiotopoulos, K. Ladomenou, D. Sun, V. Artero, A. G. Coutsolelos, *Dalton Trans.* **2016**, *45*, 6732.
[61] T. Banerjee, F. Haase, G. Savasci, K. Gottschling, C. Ochsenfeld, B. V. Lotsch, *J. Am. Chem. Soc.* **2017**, *139*, 16228.
[62] D. Vasudevan, H. Wendt, *J. Electroanal. Chem.* **1995**, *392*, 69.
[63] L. Ye, J. Liu, Y. Gao, C. Gong, M. Addicoat, T. Heine, C. Wöll, L. Sun, *J. Mater. Chem. A* **2016**, *4*, 15320.
[64] Y. Pan, J. Wang, S. Chen, W. Yang, C. Ding, A. Wasim, H.-L. Jiang, *Chem. Sci.* **2022**, *13*, 6696.
[65] Y. Sun, X. Yan, *Sol. RRL* **2017**, *1*, 1700002.
[66] J. Liu, C. Wöll, *Chem. Soc. Rev.* **2017**, *46*, 5730.
[67] B. Rausch, M. D. Symes, G. Chisholm, L. Cronin, *Science* **2014**, *345*, 1326.